Journal of Polymers and the Environment (2023) 31:3907–3924
https://doi.org/10.1007/s10924-023-02869-z

ORIGINAL PAPER

An Eco-friendly Adsorbent of Chitosan/Montmorillonite/Algae for Removal of Basic Green 1 and Reactive Blue 19 Dyes: Box-Behnken Design Optimization Mechanistic Study

Kamaliah Rosli[1] · Ahmed Saud Abdulhameed[2,3] · S. N. Surip[1,4] · Zeid A. ALOthman[5] · Ali H. Jawad[1]

Accepted: 3 April 2023 / Published online: 19 April 2023

Abstract

In this study, a green and effective adsorbent of chitosan/montmorillonite/algae (CHI/MMT/ALG) composite was developed to be an alternative adsorbent to remove dyestuffs including basic green 1 (BG1) and reactive blue 19 (RB19) from the aqueous solutions. The physicochemical characteristics of CHI/MMT/ALG were analyzed using XRD, CHN–O, BET, FTIR, pH_{pzc}, and SEM analytical techniques. The findings of the characterization revealed that the increased surface functionalities offered an enticing platform for the improved adsorption of cationic and anionic dye molecules. The essential adsorption variables, such as A: CHI/MMT/ALG dosage (0.02–0.08 g), B: pH (4–9), and C: duration (5–30 min), were optimized using the Box-Behnken design (BBD) approach. The BG1 adsorption process demonstrated a better match with the Langmuir model, whereas the RB19 adsorption process exhibited a better fit with both the Temkin and Langmuir models. The fitting of the kinetic analysis illustrates that the BG1 and RB19 adsorption by CHI/MMT/ALG could be better represented by a pseudo-second-order model. The maximum adsorption capacity of CHI/MMT/ALG for BG1 and RB19 was specified to be 509.5 mg/g and 227.9 mg/g, respectively. The endothermicity and spontaneity of the BG1 and RB19 adsorption processes are evidenced by thermodynamic analysis. The improved surface functionalities of CHI/MMT/ALG inspired the adsorption mechanism of CHI/MMT/ALG for BG1 and RB19 could be essentially ascribed by electrostatic attraction, n-π stacking, and hydrogen bonding. Overall, the study's findings indicate that the newly developed CHI/MMT/ALG has significant potential for the removal of synthetic dye from aqueous.

Keywords Chitosan · Montmorillonite · Algae · Adsorption · Organic dyes · Box-Behnken design

Introduction

The release of synthetic dyes into aquatic environments is considered one of the enormous pollution resources since they constitute a significant component of hazardous effluents. These dyes are often complex organic compounds with a variety of diverse structural configurations that are extremely stable and even resistant to biological, photolytic, and chemical activities [1]. The aquatic ecology and human health are all seriously threatened by dyes, which are often hazardous, mutagenic, and carcinogenic [2, 3]. Basic green 1(BG1) dye is primarily used in the manufacture of cover paper [4] and is also used in the textile, rubber, and plastic industries [5]. The hazardous, mutagenic, and carcinogenic effects of BG1 dye threaten aquatic species as well as humans [5]. Reactive blue 19 (RB19) dye is a toxic anionic dye that is commonly employed as a foundational ingredient in the production of polymeric dyes. It

---

✉ Ali H. Jawad
ali288@uitm.edu.my; ahjm72@gmail.com

[1] Faculty of Applied Sciences, Universiti Teknologi MARA, 40450 Shah Alam, Selangor, Malaysia

[2] Department of Medical Instrumentation Engineering, Al-Mansour University College, Baghdad, Iraq

[3] College of Engineering, University of Warith Al-Anbiyaa, Karbala, Iraq

[4] School of Computing, Engineering and Mathematical Sciences, La Trobe University, Bendigo, VIC 3552, Australia

[5] Chemistry Department, College of Science, King Saud University, Riyadh 11451, Saudi Arabia

is regarded as an organopollutant that is recalcitrant and harms both humans and other living things [6]. Therefore, reliable techniques are essential for the effective removal of organic dyes from a variety of contaminated surface waters. A variety of physical, chemical, and bioremediation methods have been developed for this purpose, including ultrafiltration [7], coagulation [8], adsorption [9], photocatalytic degradation [10], and biodegradation [11]. The adsorption procedure has been presented as a more cost-effective and efficient approach for treating organic dyes since the majority of current treatment strategies are quite expensive and generate by-pollutants [12].

From this perspective, biopolymers have appeared as environmentally friendly, cost-effective, and sustainable materials for dye removal [13]. Chitosan (CHI), the second most prevalent polymer in the environment following cellulose, is a linear polysaccharide with distinctive chemical, physical, and biological properties that commercial polymers frequently lack [14]. It offers the characteristics needed for generating effective and feasible adsorbents for environmental remediation because it is non-toxic, renewable, profuse in the functional groups, cost-effective, and ecologically friendly biopolymer [15]. Nevertheless, CHI has certain drawbacks, including limited mechanical characteristics, low surface area, and pH dependence (solubilized or viscous state in acidic media) [16]. The physicochemical characteristics of CHI have been improved through the application of techniques such as grafting [17], crosslinking [18], and composition [19], resulting in the development of a new adsorbent with desirable properties. Adsorbents with good binding strength for cationic and anionic organic dyes are subjected to several parameters such as the adsorbent's functional groups, surface area, and surface charge. For this reason, a number of unique metal oxides and natural substances have been incorporated with CHI polymer, for instance, zinc oxide [20], montmorillonite (MMT) mineral [21], and algae (ALG) biomass [22].

MMT is among the numerous and frequently utilized inorganic minerals as an efficient adsorbent for the capture of organic/inorganic contaminants from the aquatic environment owing to its unique characteristics such as high cation exchange capacity, swelling property, large specific surface area, structural stability, environment benign, and inexpensive [23–25]. As a result, it has been extensively researched that the combination of CHI biopolymer and MMT mineral is a perfect absorbent that can remove both cationic and anionic pollutants along with addressing some of CHI's drawbacks [26, 27].

In the same scenario, there has been a lot of interest in the application of biomaterials as efficient, affordable, and sustainable biosorbents (such as microalgae, fungi, and bacteria) for the removal of various pollutants from wastewater [28–30]. Due to its renewable nature, low cost, year-round availability, excellent adsorption affinity, and fairly high surface area, algae (ALG) is one of the fascinating biomaterials utilized as biosorbent for environmental remediation. ALG is known for having reactive functional groups in their structure, such as phosphate ($–PO_4^{-3}$), carboxyl (–COOH), hydroxyl (–OH), and amino ($–NH_2$) groups [31]. These groups have the ability to bind with various organic and inorganic contaminants through complexation, electrostatic attraction, and ion exchange [31]. Hence, this work attains to develop an adsorbent capable of adsorption both cationic and anionic dyes, where chitosan is basic for the adsorption of anionic dye (reactive blue 19, RB19) owing to the presence of cationic groups (e.g., $–NH_3^+$) in its backbone, while algae and montmorillonite are the basic for adsorption of cationic dye (basic green 1, BG1) owing to the presence the negatively functional groups ($PO_4^{-3}, \equiv Si-O^-, -COO^-$, and $-O^-$) in their backbone. The physicochemical properties of CHI/MMT/ALG were investigated using XRD, CHN–O, BET, FTIR, pH_{pzc}, and SEM techniques. The Box-Behnken design (BBD) strategy was used to optimize the important adsorption factors, such as A: CHI/MMT/ALG dose (0.02–0.08 g), B: pH (4–9), and C: time (5–30 min). The BG1 and RB19 dyes' experimental adsorption data were examined using kinetic, isotherm, and thermodynamic analyses. The potential adsorption mechanism of BG1 and RB19 on CHI/MMT/ALG was proposed.

Materials and Methods

Materials

The CHI flakes (deacetylation level ≤ 75) and inorganic material (MMT) were provided by Sigma-Aldrich. The Microalgae was laboratory synthesized according to the reported method [25]. An exactly measured amount of BG1 dye ($C_{27}H_{34}N_2O_4S$; FW: 482.62; dye content ~ 90%; R&M Chemicals; Color Index Number: 42040) and RB19 ($C_{22}H_{16}N_2Na_2O_{11}S_3$; FW: 626.53 g/mol; dye content ~ 50%; R&M Chemicals; Color Index Number: 61200) was dissolved in 1 L of deionized water to obtain the stock solution (1000 mg/L). In this study, analytical-grade chemicals from R&M Chemicals, namely, HCl, NaOH pellets, and NaCl powder were used.

CHI/MMT/ALG Synthesis

The CHI/MMT/ALG's synthesis was based on the method outlined in the literature [32]. The CHI/MMT/ALG was produced by combining 2 g of CHI, 1 g of MMT, and 1 g of ALG with 80 mL of a 5% v/v solution of acetic acid under strenuously stirring for 24 h at 27 °C. A syringe needle (10 mL) was used to insert the CHI/MMT/ALG solution into a NaOH solution (0.5 M, 1000 mL) to create CHI/MMT/ALG beads. CHI/MMT/ALG beads were crushed while oven dried for 24 h after being washed with water to get rid of any NaOH residue. Finally, CHI/MMT/ALG was powdered to a tiny powder (˂250 μm) for BG1 and RB19 adsorption studies. The preparation steps of CHI/MMT/ALG are given in Fig. 1.

Characterization

The instrument (Micromeritics, ASAP 2060) was used to examine the surface physical characteristics of the CHI/MMT/ALG, including its pore volume and specific surface area. The surface configurations of the CHI/MMT/ALG were examined using scanning electron microscopy (SEM, Zeiss Supra 40 VP) prior to and following the adsorption of RB19 and BG1. The samples were put on stubs, coated with gold using a gold-coating device, and then SEM analysis was performed at 15.0 keV to provide high-resolution SEM micrographs. The crystalline nature of CHI/MMT/ALG was identified using an X-ray polycrystal diffractometer (XRD, PANalytical X'Pert PRO). Fourier transform infrared (FTIR) spectra from the FTIR spectrophotometer (Perkin-Elmer, Spectrum RX I) were taken to describe the essential groups of CHI/MMT/ALG before and after the adsorption of RB19 and BG1. The charge on the CHI/MMT/ALG surface was derived using a point of zero charge (pH_{pzc}) procedure [33]. The proportions of carbon (C), hydrogen (H), nitrogen (N), and oxygen (O) in CHI/MMT/ALG were measured using a CHN–O analyzer (Flash 2000, Thermo-Scientific).

Experimental Design

The optimal conditions of three input factors (CHI/MMT/ALG dosage, pH, and duration), which result in maximum BG1 and RB19 adsorption onto CHI/MMT/ALG were identified using BBD. Adsorption experiments were built using Design Expert (13.0, Stat-Ease, USA), and the outcomes were statistically analyzed. Table 1 presents three studied factor ranges (i.e., 1, 0, and 1): CHI/MMT/ALG dosage (A), pH (B), and time (C). The experimental design's ranges for each variable studied were determined based on the findings of premonitory investigations. Two replication runs (experiments) were done under the same conditions for each test, and the findings are provided as an average. The following equation (Eq. (1), 2nd polynomial) was used to predict the relationship between the dependent variable and the independent variables in order to determine the best operational parameters [19].

$$Y = \beta_0 + \sum_{i=1}^{k} \beta_i X_i + \sum_{i=1}^{k} \beta_{ii} X_i^2 + \sum_{i=1}^{k} \sum_{j=1}^{k} \beta_{ij} X_i X_j + \varepsilon \tag{1}$$

where Y = response (dye removal); β_i = linear influence; β_0 = intercept; β_{ij} = interaction effect; and X_i and X_j

Table 1 Codes and actual variables and their levels in BBD

Codes	Variables	Level 1 (− 1)	Level 2 (0)	Level 3 (+ 1)
A	Dose (g)	0.02	0.05	0.08
B	pH	4	6.5	9
C	Time (min)	5	17.5	30

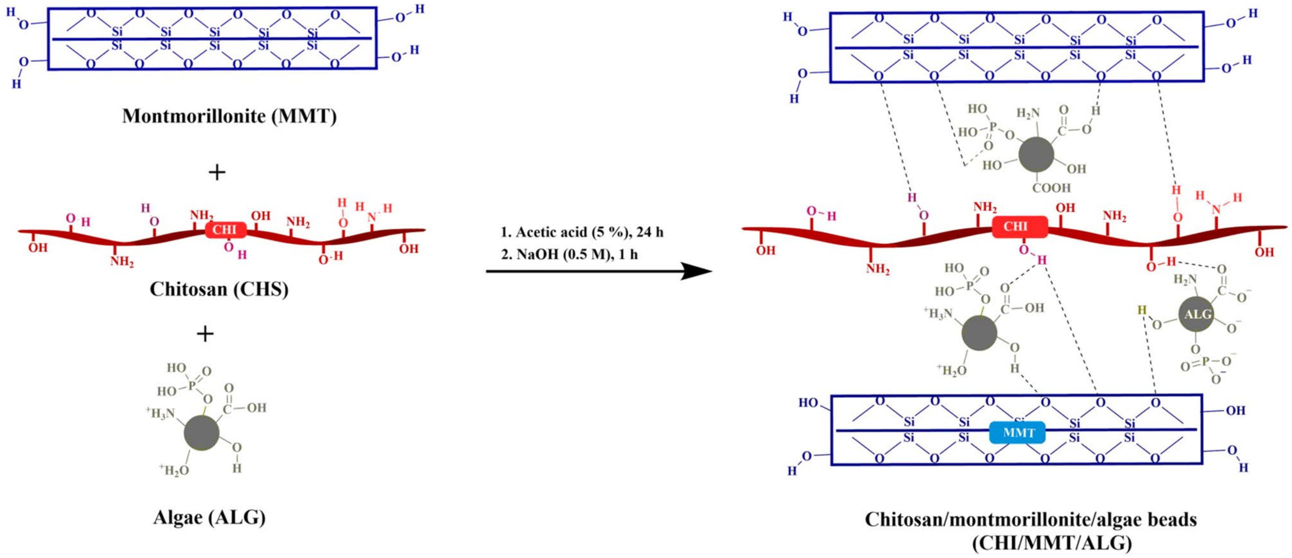

Fig. 1 The preparation steps of CHI/MMT/ALG

= independent variables. K and ε represent the number of parameters and the random error discrepancies, respectively. Table 2 outlines the functions of generated models as well as actual responses (BG1 removal and RB19 removal). In order to begin the BG1 and RB19 decolorization tests, a specific amount of CHI/MMT/ALG was introduced to Erlenmeyer flasks having dye solution (100 mL). The solutions were moved into a water-bath thermostatic oscillator (WNB7-45, Memmert) and quietly agitated for a determined time period at a constant rate of 90 rpm. The solutions were then filtered through a 0.45 µm syringe filter (evergreen, 25 mm Nylon for BG1 dye; 25 mm PTFE hydrophobic for RB19 dye) to obtain liquids free of CHI/MMT/ALG. By using a spectrophotometer (HACH DR 3900) the remnant concentration in the BG1 and RB19 solutions was detected at $\lambda_{max} = 625$ nm and $\lambda_{max} = 592$ nm, respectively. The next formula (2) was employed to measure the removal effectiveness ($R\%$) of BG1 and RB19 dyes [12]:

$$R\% = \frac{\left(C_o - C_e\right)}{C_o} \times 100 \tag{2}$$

where C_o (mg/L) and C_e (mg/L) indicate the adsorbates' concentrations in the beginning and equilibrium levels, respectively.

Table 2 Experimental matrix based on BBD approach for designing experiments and corresponding responses (BG1 removal (%) and RB19 removal (%)

Run	A: Dose (g)	B: pH	C: Time (min)	BG1 removal (%)	RB19 removal (%)
1	0.02	4	17.5	6.2	54.7
2	0.08	4	17.5	21.7	91.7
3	0.02	9	17.5	28.9	41.2
4	0.08	9	17.5	76.2	61.1
5	0.02	6.5	5	19.7	33.8
6	0.08	6.5	5	67.6	46.6
7	0.02	6.5	30	64.1	38.2
8	0.08	6.5	30	73.2	80.9
9	0.05	4	5	9.7	66.1
10	0.05	9	5	56.4	34.3
11	0.05	4	30	27.1	77.8
12	0.05	9	30	68.9	63.1
13	0.05	6.5	17.5	49.5	52.5
14	0.05	6.5	17.5	46.6	55.4
15	0.05	6.5	17.5	40.4	57.9
16	0.05	6.5	17.5	47.2	54.9
17	0.05	6.5	17.5	48.8	50.8

Adsorption Study of BG1 and RB19 on CHI/MMT/ALG

Batch adsorption procedures have been used to determine the maximum quantity of adsorbate that can adsorb onto the CHI/MMT/ALG. Based on the BBD model, maximum removals of 76.2% and 91.7% were attained at CHI/MMT/ALG dosage of 0.08 g, pH of 9 for BG1 and 4 for RB19, and duration of 17.5 min for BG1 and RB19, respectively. With these ideal input factors, a range of BG1 and RB19 concentrations (20–250 mg/L) were tested for adsorption equilibrium. BG1 and RB19 batch adsorption tests were conducted using the same approach described in the previous "Experimenta design". The equilibrium adsorption capacity (q_e, mg/g) of the CHI/MMT/ALG was established using the formula (3) as follows [12]:

$$q_e = \frac{\left(C_o - C_e\right)V}{W} \tag{3}$$

where W (g) signifies the CHI/MMT/ALG's quantity and V (L) denotes the dye solution volume.

Results and Discussion

Characterization of CHI/MMT/ALG

The CHI/MMT/ALG's surface area and porosity are indispensable characters for the adsorption of the RB19 and BG1 dyes. Table 3 records elemental analysis and the surface characteristics of CHI/MMT/ALG. The percentages of C, H, N, and O in CHI/MMT/ALG were 31.94%, 5.26%, 5.72%, and 57.08, respectively, as shown by elemental analyzed data. The calculated pore volume and surface area of CHI/MMT/ALG are 0.01029 cm^3/g and 2.64 m^2/g, respectively. The measurements of the mean pore diameter (14.80 nm) show that the CHI/MMT/ALG has a mesoporous structure [pores varying in size (2.0–50 nm)] as per IUPAC [34]. The CHI/MMT/ALG's N_2 adsorption/desorption isotherms are represented in Fig. 2. As per the IUPAC classification, the

Table 3 Physiochemical characteristics of CHI/MMT/ALG

Parameter(s)	CHI/MMT/ALG
Surface area (m^2/g)	2.64
Langmuir surface area (m^2/g)	3.0683
Pore volume (cm^3/g)	0.01029
Mean pore diameter (nm)	14.80
C (%)	31.94
H (%)	5.26
N (%)	5.72
O (by the difference) (%)	57.08

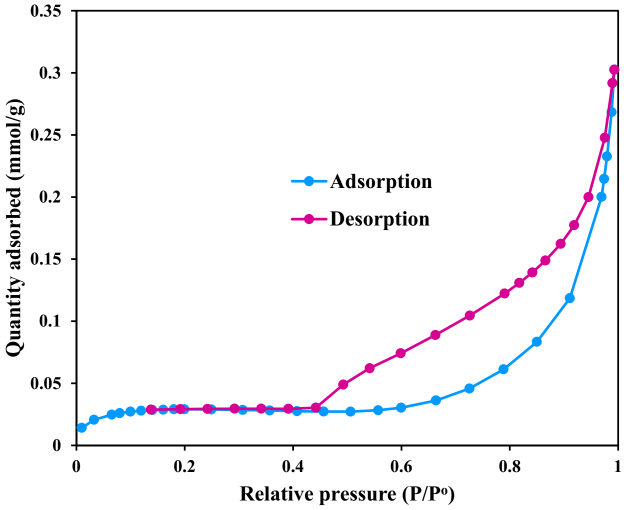

Fig. 2 The N_2 adsorption–desorption isotherms of CHI/MMT/ALG

CHI/MMT/ALG's N_2 adsorption/desorption isotherms were type IV, which supports the existence of mesopores [34]. The type H3 hysteresis loop depicted in Fig. 2 confirms the existence of mesopores in the CHI/MMT/ALG [35].

The XRD study was conducted to identify the crystalline phase of the powdered CHI/MMT/ALG. The CHI/MMT/ALG's XRD pattern appears in Fig. 3. XRD analysis of CHI shows a prominent peak at about $2\theta = 20°$, which is characteristic of the quasi-crystalline phase of CHI [36]. The crystalline phase of cellulose associated with ALG may also be deduced from the unique peak at 22° [37]. Importantly, XRD pattern of CHI/MMT/ALG exhibited several peaks at $2\theta = 9°$, 18°, 19.8°, 27.5°, and 36°, which correspond to the (001), (002), (020), (003), and (130) planes of MMT, respectively [1].

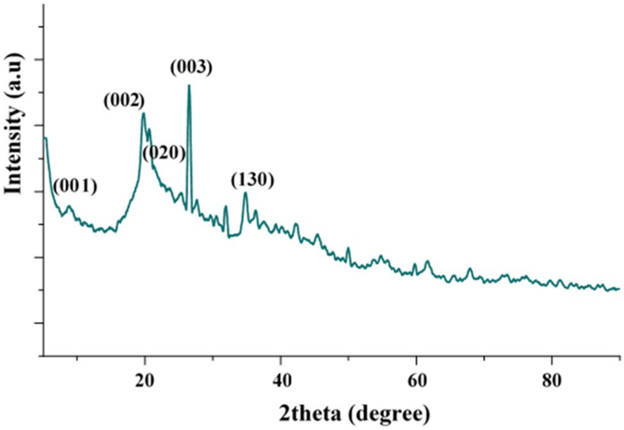

Fig. 3 XRD pattern CHI/MMT/ALG

FTIR spectroscopy analysis was used to fully identify the functional groups available in the CHI/MMT/ALG prior to and after the adsorption of the adsorbates (BG1 and RB19). The FTIR spectra of (a) CHI/MMT/ALG before and after (b) BG1 and (c) RB19 adsorption appear in Fig. 4. The O–H stretching vibrations of the MMT, CHI, and ALG are accountable for the absorption bands in the 3300–3650 cm^{-1} range that are seen in the CHI/MMT/ALG spectra (Fig. 4a) [38]. The stretching vibrations of amino ($-NH_2$) groups, which are associated with CHI and ALG biomaterials, are also shown by this bandwidth [1]. The C-H stretching vibrations in the alkyl chain caused the band at 2850 cm^{-1} to arise [29]. Furthermore, there were many peaks at 2300 cm^{-1}, 1650 cm^{-1}, 1500 cm^{-1}, and 1360 cm^{-1}, which correspond to the C≡C bonds, carbonyl C=O groups, the stretching vibration of the C=C bonds, and the C-N stretching (present in the amino functional groups of CHI and ALG), respectively. The Si–O

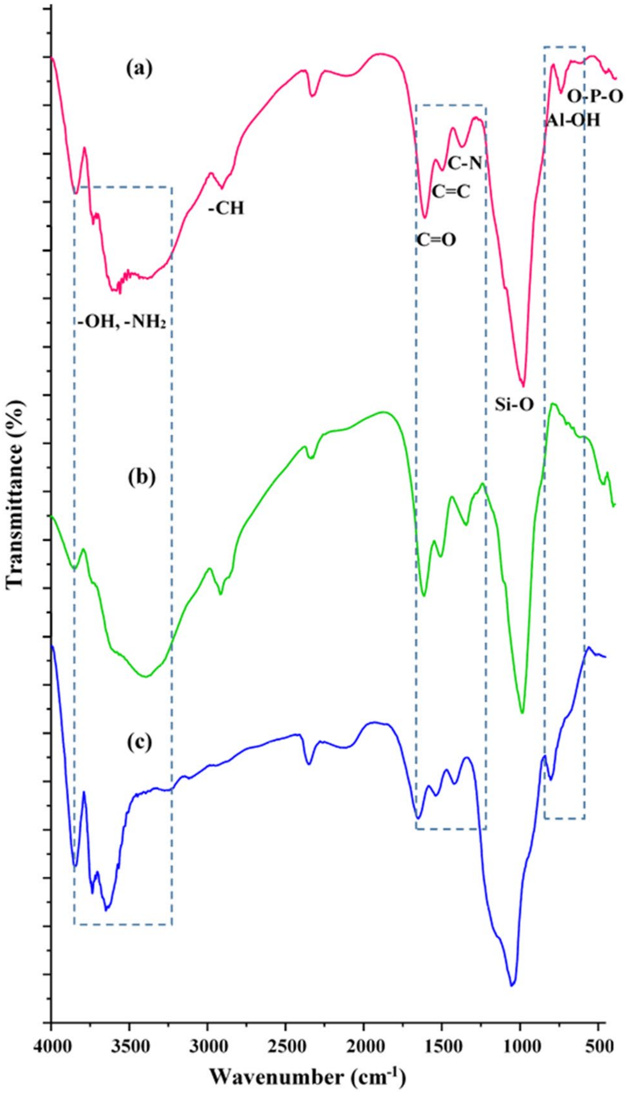

Fig. 4 FTIR spectra of (a) CHI/MMT/ALG and CHI/MMT/ALG after adsorption (b) BG1 and (c) RB19 dyes

stretching vibration of the Si–O–Si bonds in the tetrahedral layer causes the strong band detected at 1022 cm^{-1} [38]. The vibrations of the Al–OH bond (MMT) and the O–P–O bond (ALG) were linked to the absorption peaks at 720 cm^{-1} and 545 cm^{-1}, respectively [39]. The FTIR spectra of CHI/MTT/ALG after BG1 and RB19 adsorption displayed spectra that were substantially similar to CHI/MMT/ALG with alterations in various bands (e.g., absorption peaks of -OH, $-NH_2$, C=O, and peak Al–OH), stating that the reactive groups of CHI/MMT/ALG played a major role in BG1 and RB19 adsorption.

Prior to and during the uptake of the adsorbates (BG1 and RB19), the surface morphologies of CHI/MMT/ALG were examined by SEM analysis. Figure 5a–c presents the microphotographs of the SEM analysis for CHI/MMT/ALG before and after the adsorption of the adsorbates (BG1 and RB19). As shown in Fig., the surface of CHI/MMT/ALG is uneven, diverse, and contains some cracks. The morphology

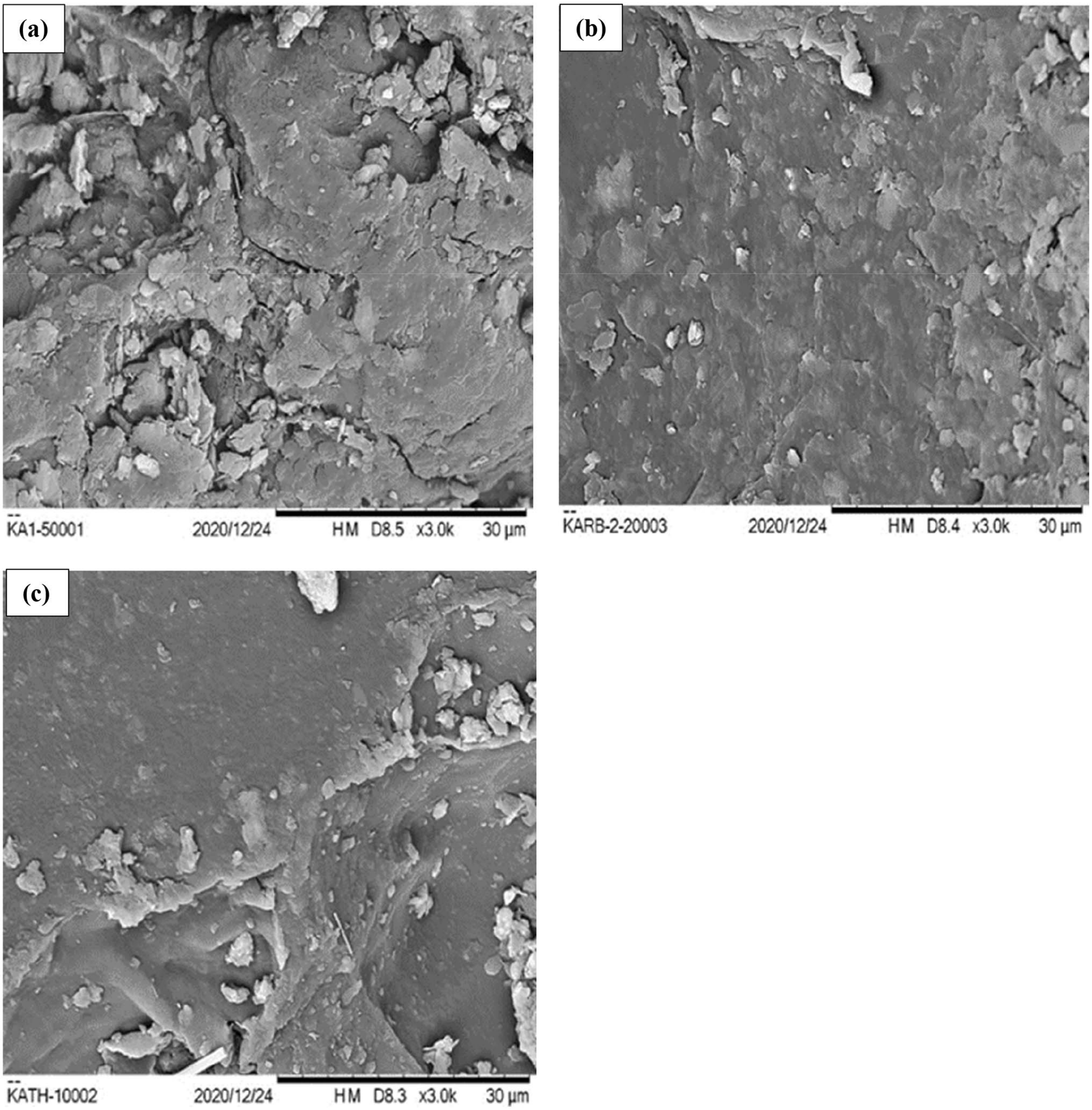

Fig. 5 SEM images and EDX spectra of (**a**) CHI/MMT/ALG, (**b**) CHI/MMT/ALG after RB19 adsorption, and (**c**) CHI/MMT/ALG after BG1 adsorption

of CHI/MMT/ALG was slightly changed after the adsorption of BG1 (Fig. 5b) and RB19 (Fig. 5c), in accordance with the adsorption of BG1 and RB19 molecules on the CHI/MMT/ALG surface.

Statistical Evaluation

The relationship between the hypothesized and actual data, as well as the accuracy of the developed 2nd mathematical model, were assessed using ANOVA. Table 4 summarizes the statistics of the ANOVA for the BG1 and RB19 removals. The BG1 removal and RB19 removal had F-values of 49.40 and 102.73, respectively, implying that the models could be applied to evaluate the relationship between the theoretical and experimental findings [40]. The strong correlation coefficients of BG1 removal ($R^2 = 0.984$) and RB19 removal ($R^2 = 0.992$) highlighted the significance of the models and the fact that the estimated and actual removal measurements of BG1 and RB19 dyes are perfectly consistent. The minimal p-values (Lack of Fit), 0.2847 and 0.9778 for BG1 removal and RB19 removal, respectively, supported the robustness of the predicted models [41]. If $p < 0.05$, the properties of the suggested model are assumed to be statistically significant. The removal of BG1 is mathematically influenced by the following terms: A, B, C, AB, AC, B^2, and C^2, while the removal of BG1 is mathematically influenced by the following terms: A, B, C, AB, AC, BC, B^2, and C^2. The BG1 removal and RB19 removal quadratic Eqs. (4) and (5) were developed by calculating the most important input factors.

$$\text{BG1 removal}(\%) = +46.50 + 14.98A + 20.71B + 9.99C + 7.95AB - 9.70AC - 14.44B^2 + 8.46C^2 \tag{4}$$

$$\text{RB19 removal}(\%) = +54.30 + 14.05A - 11.32B + 9.90C - 4.28AB + 7.48AC + 4.28BC + 9.16B^2 - 3.14C^2 \tag{5}$$

Figure 6a and b provide the normal probabilities for the BG1 removal and RB19 removal models, respectively. The spots in Figs. 5a and b seem to be closely matched to a single line, supporting the suitability and acceptability of the models and the ANOVA statistics [42]. Figure 6c and d provide graphics illustrating the link between the expected and actual levels of BG1 and RB19 removals. In Fig. 6c and d, the significant association between the observed outcomes (BG1 removal and RB19 removal) and those that are hypothetically calculated are evident, proving the statistical validity of the designed models. The plots of the residuals versus the run number are represented in Fig. 6e and f. The accuracy of the models is also evidenced by the points' random distribution around zero in Fig. 6e and f.

Interactive Effects of Factors

In order to assess the impact of the investigated factors and to identify the significant relationships between the tested characteristics on the BG1 and RB19 removal processes, 3D response surface diagrams were constructed. Figure 6a and b express the dual influences of the CHI/MMT/ALG dosage and pH on the rate of removal of BG1 and RB19 whereas the time (17.5 min)

Table 4 ANOVA analysis for BG1 removal (%) and RB19 removal (%)

	BG1 removal (%)					RB19 removal (%)				
Source	Sum of Squares	df	Mean Square	F-value	p-value	Sum of Squares	df	Mean Square	F-value	p-value
Model	7790.49	9	865.61	49.40	< 0.0001	4146.15	9	460.68	102.73	< 0.0001
A-Dose	1794.01	1	1794.01	102.37	< 0.0001	1579.22	1	1579.22	352.17	< 0.0001
B-pH	3432.06	1	3432.06	195.85	< 0.0001	1026.04	1	1026.04	228.81	< 0.0001
C-Time	798.00	1	798.00	45.54	0.0003	784.08	1	784.08	174.85	< 0.0001
AB	252.81	1	252.81	14.43	0.0067	73.10	1	73.10	16.30	0.0049
AC	376.36	1	376.36	21.48	0.0024	223.50	1	223.50	49.84	0.0002
BC	6.00	1	6.00	0.3425	0.5767	73.10	1	73.10	16.30	0.0049
A^2	5.94	1	5.94	0.3388	0.5788	6.98	1	6.98	1.56	0.2523
B^2	877.65	1	877.65	50.08	0.0002	353.48	1	353.48	78.83	< 0.0001
C^2	301.53	1	301.53	17.21	0.0043	41.45	1	41.45	9.24	0.0188
Residual	122.67	7	17.52			31.39	7	4.48		
Lack of Fit	70.67	3	23.56	1.81	0.2847	1.37	3	0.4567	0.0608	0.9778
Pure Error	52.00	4	13.00			30.02	4	7.50		
Cor Total	7913.16	16				4177.54	16			

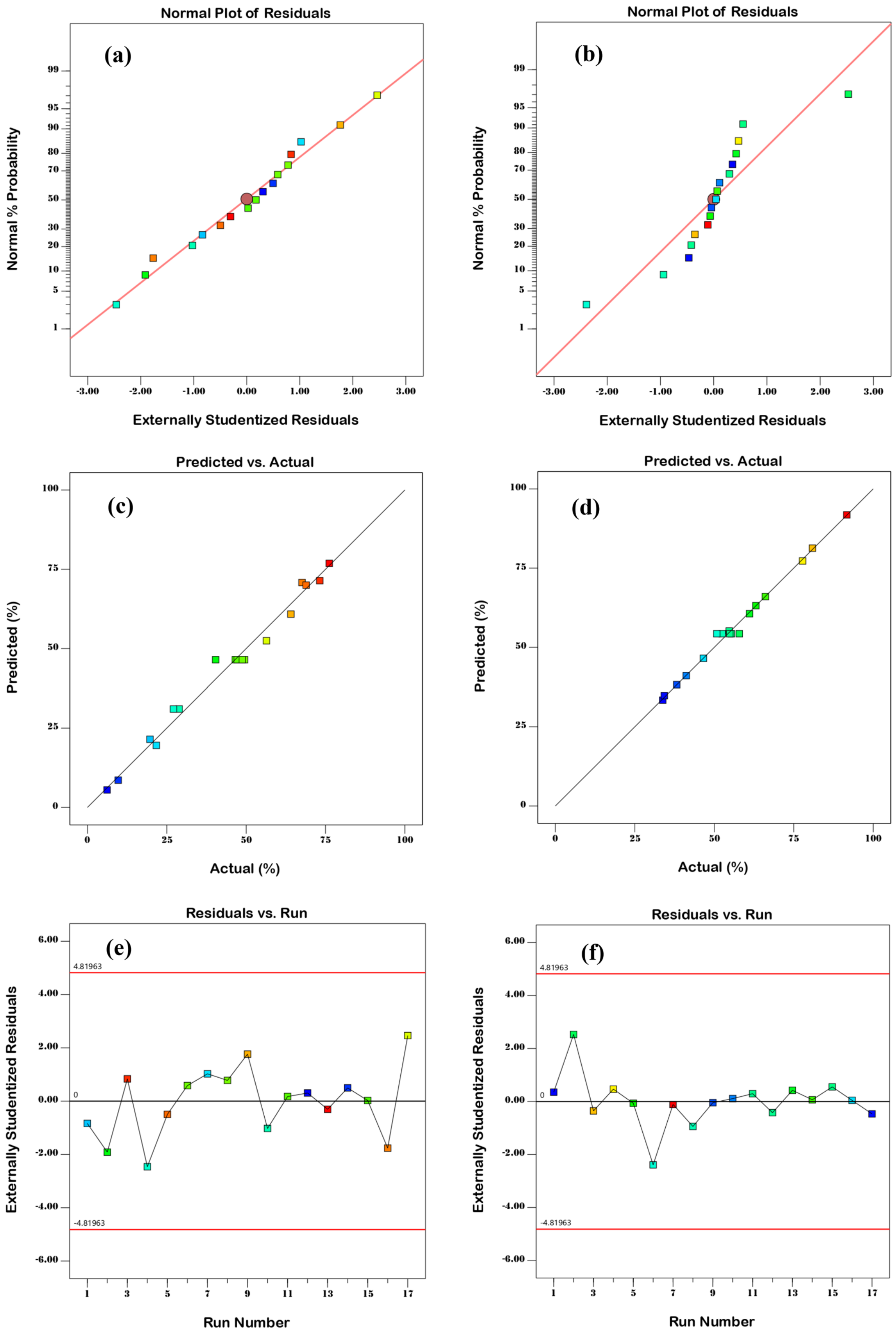
Normal Plot of Residuals
(a)
Normal % Probability
99
95
90
80
70
50
30
20
10
5
1
-3.00
-2.00
-1.00
0.00
1.00
2.00
3.00
Externally Studentized Residuals
Normal Plot of Residuals
(b)
Normal % Probability
Externally Studentized Residuals
Predicted vs. Actual
(c)
Predicted (%)
100
75
50
25
0
Actual (%)
Predicted vs. Actual
(d)
Predicted (%)
Actual (%)
Residuals vs. Run
(e)
Externally Studentized Residuals
6.00
4.00
2.00
0.00
-2.00
-4.00
-6.00
4.81963
0
-4.81963
1
3
5
7
9
11
13
15
17
Run Number
Residuals vs. Run
(f)
Externally Studentized Residuals
4.81963
0
-4.81963
Run Number

◂**Fig. 6** **a** Normal probability plots of residuals for (**a**) BG1 and (**b**) RB19; plots of the relationship between the predicted and actual values of (**c**) BG1 and (**d**) RB19; plots of the residual versus run number of (**e**) BG1 and (f) RB19

was held unchanged. It is evident from the results shown in Fig. 7a and b that the adsorption efficiency of BG1 and RB19 was significantly improved at pH 9 and 4, respectively. As shown in Fig. 7b, the effectiveness of RB19 removal was enhanced by increasing CHI/MMT/ALG dosages synchronized with lowering pH. Analyzing the impact of pH on BG1 and RB19 adsorption could be done using the pH_{pzc} property of CHI/MMT/ALG and the favored form (anionic or cationic) of the adsorbates (BG1/RB19) to CHI/MMT/ALG surface. According to Fig. 7f, CHI/MMT/ALG had a $pH_{pzc} = 7.5$. In turn, this caused the CHI/MMT/ALG surface to change from positively charged to negatively charged for basic pH values over pH_{pzc}, and vice versa at acidic pH values (i.e., from positively charged to negatively charged). This increases CHI/MMT/ALG's concentration on adsorbing positively charged MB molecules and negatively charged RB19 molecules depending on pH value, as illustrated in the formulas below (Eq. (6) and (7)).

$$\text{CHI/MMT/ALG}^{-} + \text{BGI}^{+} \leftrightarrow \text{CHI/MMT/ALG}^{-}\ldots{}^{+}\text{BGI} \tag{6}$$

$$\text{CHI/MMT/ALG}^{+} + \text{RB19}^{-} \leftrightarrow \text{CHI/MMT/ALG}^{+}\ldots{}^{-}\text{RB19} \tag{7}$$

Figure 7c and d, respectively, demonstrate the dual influences of the CHI/MMT/ALG dosage and time on the removal rates of BG1 and RB19, whereas pH (6.5) was kept unchanged. The data displayed in Fig. 6c demonstrate that elevating the dose of CHI/MMT/ALG from 0.02 g to 0.08 g boosted the efficacy of removing BG1, but did not improve the efficacy of removing RB19 synchronized with extending the time. The increased BG1 removal is ascribed to the CHI/MMT/ALG's large surface area and efficient adsorption sites at higher CHI/MMT/ALG dosages. As per Fig. 7c, the level of BG1 removal improved with extending the time (30). This happens because the BG1 molecules require considerable time to enter the CHI/MMT/ALG pores, attach to the surface of the CHI/MMT/ALG, and attain the equilibrium time. Figure 7e illustrates the combined impact of pH and time on the rate of RB19 removal while maintaining a consistent dosage of CHI/MMT/ALG (0.05 g). Figure 7e exhibits that the RB19 dye's adsorption efficiency was increased at an adsorption duration of 30 min. This observation is linked that RB19 molecules needing sufficient time to penetrate the CHI/MMT/ALG pores, attach to the surface of the CHI/MMT/ALG, and achieve the equilibrium time.

Adsorption Study

Examining the impact of initial dye concentration is necessary to fully understand the adsorption performance characteristics of the CHI/MMT/ALG and the nature of relations between CHI/MMT/ALG and dye species. As demonstrated in Fig. 8a, b, varying the initial concentration (20–250 mg/L) of the BG1 and RB19 solutions possesses a remarkable impact on the adsorption efficiency of the CHI/MMT/ALG. The effect of initial concentration was investigated using 100 mL of dye solution and 0.08 g/L of CH/MMT/ALG at 30 °C and pH (9 for BG1 and 4 for RB19). The adsorption rate of CHI/MMT/ALG was significantly enhanced (41.31 to 330.08 mg/g for BG1; 20.04 to 226.70 mg/g for RB19) when the initial concentration of BG1 and RB19 was changed from 20 to 250 mg/L. This increment can be due to a rise in the mass transfer driving force that appears when the initial concentration of the dye is raised. As a consequence of this boost in driving force, more dye molecules in the bulk solution migrate into the interior pores of the CHI/MMT/ALG [43].

Adsorption Kinetics

The information provided by the kinetic study is extremely helpful for scaling up and developing the technology of the adsorption process of BG1 and RB19 employing CHI/MMT/ALG. Two kinetic models, namely, pseudo-first-order and pseudo-second-order were applied in order to specify the adsorption process and analyze the kinetics of the BG1 and RB19 adsorption [44, 45]. For all of these models, Table 5 provides the non-linear equations of them, while Table 6 provides values of the computed kinetic parameters. The PSO model was found to have higher R^2 values than the PFO model (cf. Table 6), and the estimated values of q_e for the PSO model were notably comparable to the actual values of q_e, illustrating that the BG1 and RB19 adsorption by CHI/MMT/ALG could be better represented by a pseudo-second-order model. This finding indicates that the primary driver of the BG1 and RB19 adsorption is the chemisorption mechanism [46]. The k_2 values decrease as the initial dye concentrations increase from 20 to 250 mg/L. Lower k_2 values are a result of the longer time to equilibrium, and thus indicate a lower rate of adsorption with increase in initial dye concentrations [47].

Adsorption Isotherms

The maximum adsorptive capacity of the CHI/MMT/ALG as well as the nature of relations between CHI/MMT/ALG and dye species were evaluated using isotherm models. The Langmuir, Freundlich, and Temkin isotherms were used to thoroughly investigate the adsorption of BG1 and RB19 on

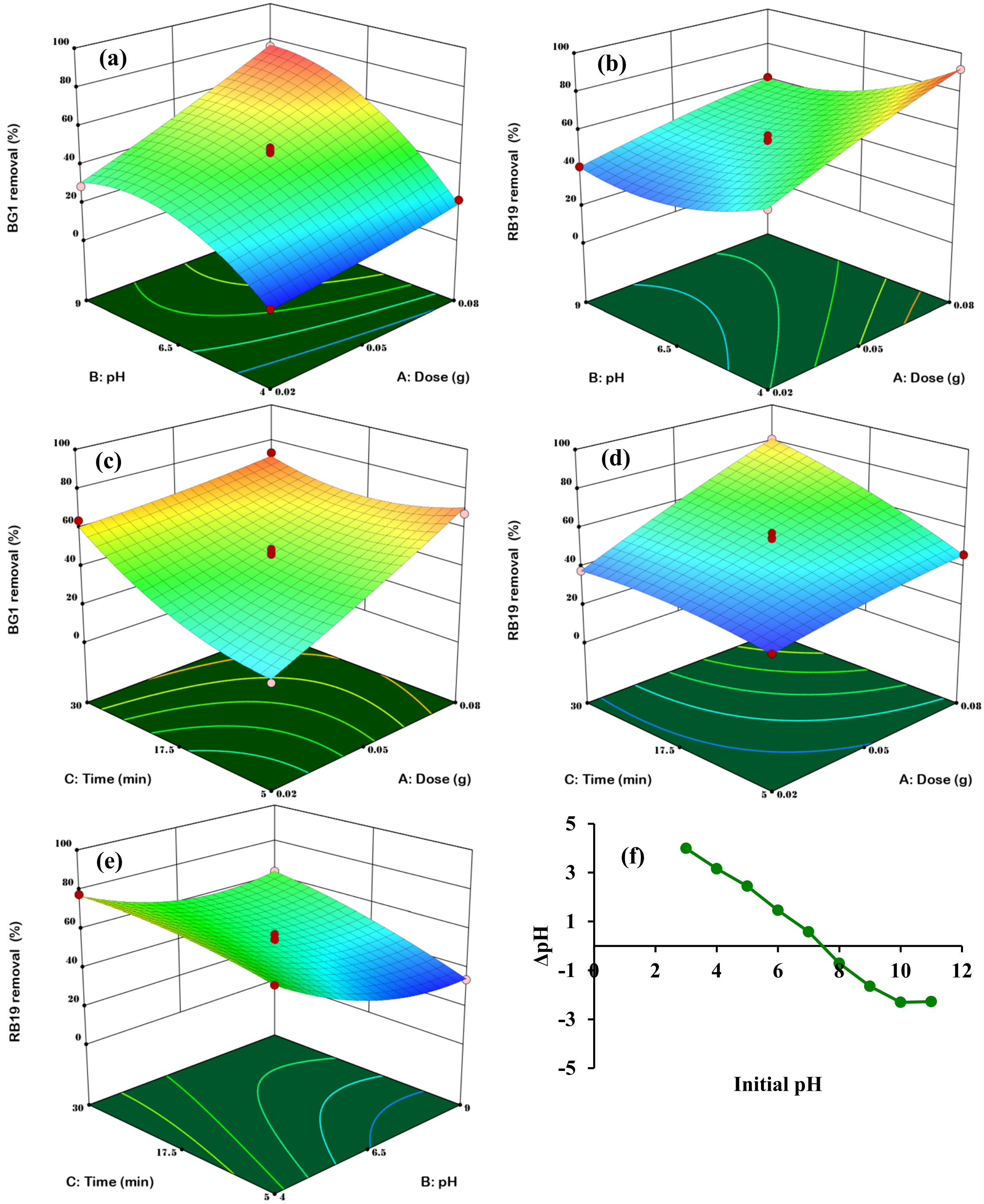

Fig. 7 3D response surfaces plots of significant interactions including (**a**) AB (dose × pH) for BG1 removal, (**b**) AB (dose × pH) for RB19 removal, (**c**) AC (dose × time) for BG1 removal, (**d**) AC (dose × time) for RB19 removal, and (**e**) BC (pH × time) for RB19 removal, while (**f**) pH$_{pzc}$ of CHI/MMT/ALG

CHI/MMT/ALG [48–50]. For all of these models, Table 5 provides the non-linear equations of them, while Table 7 and Fig. 9a, b provide values of the computed isotherm parameters and diagrams of isotherm models, respectively. As per the R^2 values outlined in Table 7, the BG1 adsorption process demonstrated a better match with the Langmuir

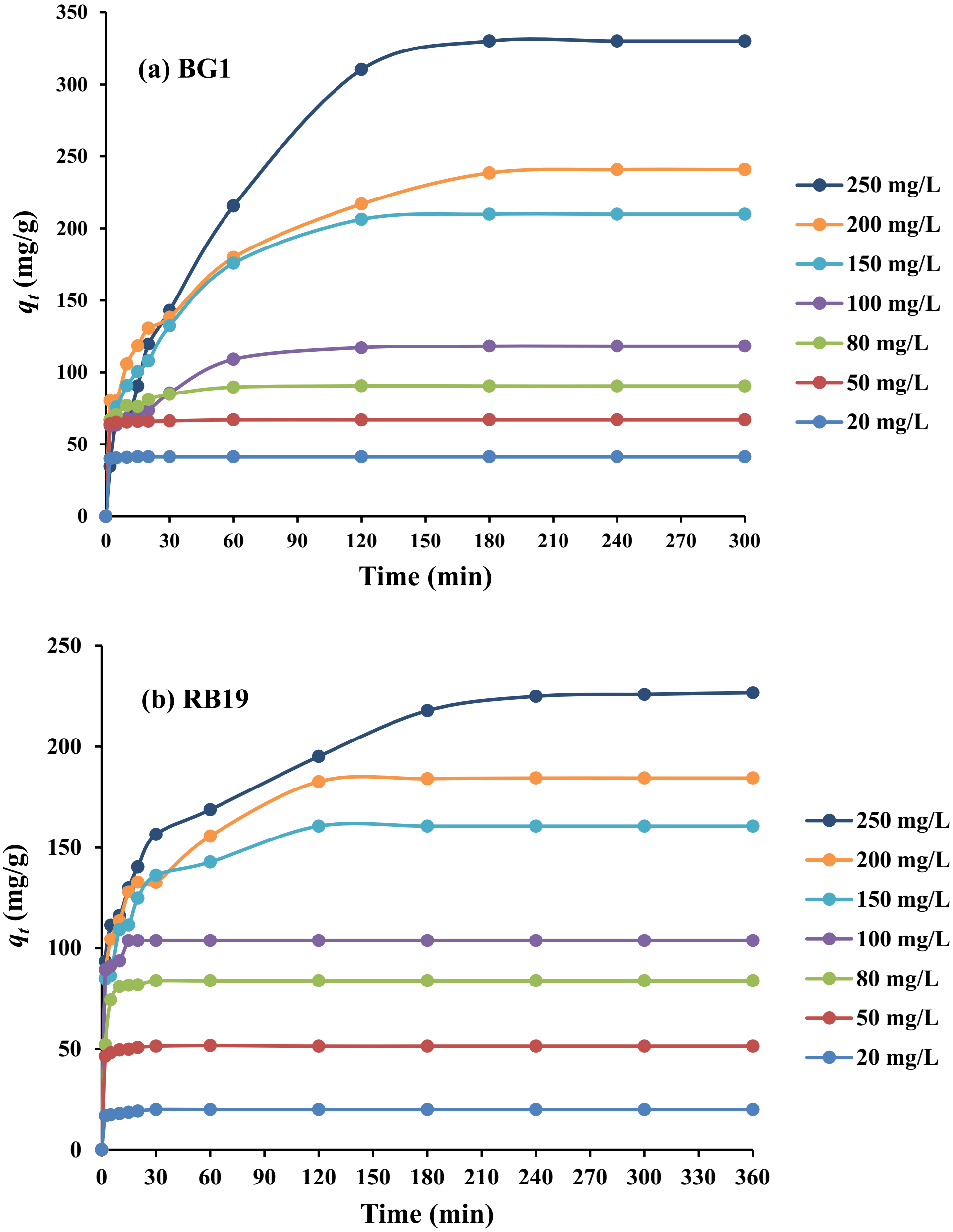

Fig. 8 Effect of the contact time on (**a**) BG1 and (**b**) RB19 adsorption at several concentrations (dosage = 0.08 g, solution pH = 9 for BG1 and 4 for RB19, temperature = 25 °C, agitation speed = 85 rpm, and volume of solution = 100 mL)

Table 5 Adsorption kinetics and isotherms nonlinear models

Models	Formula	Descriptions
Pseudo-first order (PFO)	$q_t = q_e\left(1 - e^{-k_1 t}\right)$	k_1: pseudo-first-order rate constant (1/min)
Pseudo-second order (PSO)	$q_t = \frac{q_e^2 k_2 t}{1+q_e K_2 t}$	k_2: pseudo-second-order rate constant (g/mg min)
Langmuir	$q_e = \frac{q_m K_L C_e}{1+K_L C_e}$	q_m: monolayer capacity (mg/g) K_L: Langmuir constant (L/mg)
Freundlich	$q_e = K_F C_e^{1/n}$	K_F: Freundlich constant (mg/g) (L/mg)$^{1/n}$ n: adsorption intensity
Temkin	$q_e = \frac{RT}{b_T} ln\left(K_T C_e\right)$	K_T: Temkin constant (L/mg) b_T: heat of adsorption (J/mol)

Table 6 PFO and PSO kinetic parameters for the BG1 and RB19 adsorption on CHI/MMT/ALG

BG1 Concentration (mg/L)	$q_{e\,exp.}$ (mg/gm)	PFO			PSO		
		$q_{e\,cal}$ (mg/gm)	k_1 (1/min)	R^2	$q_{e\,cal}$ (mg/gm)	$k_2 \times 10^{-2}$ (g/mg min)	R^2
20	41.3	41.2	1.806	0.99	41.3	35.89	0.99
50	67.1	66.5	1.683	0.99	66.8	16.17	0.99
80	90.5	84.8	0.688	0.94	88.2	1.277	0.98
100	118.2	110.6	0.094	0.94	114.5	0.169	0.86
150	209.8	204.1	0.046	0.91	221.4	0.0297	0.95
200	240.8	225.4	0.047	0.88	245.5	0.0150	0.93
250	330.1	333.2	0.020	0.98	400.0	0.0053	0.99
RB19 Concentration (mg/L)	$q_{e\,exp.}$ (mg/gm)	PFO			PSO		
		$q_{e\,cal}$ (mg/gm)	k_1 (1/min)	R^2	$q_{e\,cal}$ (mg/gm)	$k_2 \times 10^{-2}$ (g/mg min)	R^2
20	20.0	19.4	0.963	0.97	19.8	10.84	0.99
50	51.4	50.7	1.212	0.99	51.3	8.173	0.99
80	83.9	83.2	0.478	0.99	85.5	1.121	0.99
100	103.8	101.9	1.000	0.98	103.8	2.382	0.99
150	160.6	149.9	0.159	0.85	157.6	0.177	0.95
200	184.4	168.7	0.139	0.82	178.7	0.128	0.93
250	226.7	204.5	0.082	0.81	215.9	0.064	0.91

model, whereas the RB19 adsorption process exhibited a better fit with both the Temkin and Langmuir models. The equilibrium findings revealed that the adsorption of BG1 and RB19 happened via monolayer adsorption on the homogeneous surface of CHI/MMT/ALG [51]. Values of 1/n indicate whether an isotherm is irreversible (1/n = 0), favorable (0 > 1/n < 1 or unfavorable (1/n > 1). In the Freundlich isotherm, the values of 1/n for BG1 and RB19 were 0.56 and 0.33, demonstrating a desirable adsorption behavior [52]. Table 7 demonstrates that the b_T value is positive, demonstrating that the adsorption process is endothermic since the heat of adsorption rises with a rise in temperature [12]. The maximum adsorption capacity of CHI/MMT/ALG for BG1 and RB19 was specified to be 509.5 mg/g and 227.9 mg/g, respectively. Table 8 displays the determined adsorption capabilities of CHI/MMT/ALG as well as other adsorbent materials applied for the adsorption of BG1 and RB19. Overall, the study's findings indicate that the newly developed CHI/MMT/ALG has significant potential for employment in synthetic dye removal applications.

Table 7 The parameters of isotherm models and equilibrium parameters for BG1 and RB19 adsorption on CHI/MMT/ALG

Adsorption isotherm	Parameter	BG1	RB19
Langmuir	q_m (mg/gm)	509.5	227.9
	K_a (L/mg)	0.7912	0.28
	R^2	0.969	0.95
Freundlich	K_f (mg/gm) (L/mg)$^{1/n}$	207.84	64.58
	1/n	0.56	0.33
	R^2	0.941	0.89
Temkin	K_T (L/mg)	2.64	1.21
	b_T (J/mol)	29.21	56.0
	R^2	0.884	0.95

Thermodynamic Functions

The adsorption mode of BG1 and RB19 on CHI/MMT/ALG in terms of feasibility and spontaneity was inspected with thermodynamic features including change in Gibbs free energy (ΔG°), entropy (ΔS°), enthalpy (ΔH°) at four different temperatures, 303.15 K, 313.15 K, 323.15 K, and 333.15 K. The Gibbs Eq. (8), thermodynamic equilibrium constant (k_d) Eq. (9), and Van't Hoff Eq. (10) were used to extract the ΔG◦, k_d, and ΔH° and ΔS°), respectively [61].

$$\Delta G^\circ = -RTlnk_d \tag{8}$$

$$k_d = \frac{q_e}{C_e} \tag{9}$$

$$lnk_d = \frac{\Delta S^\circ}{R} - \frac{\Delta H^\circ}{RT} \tag{10}$$

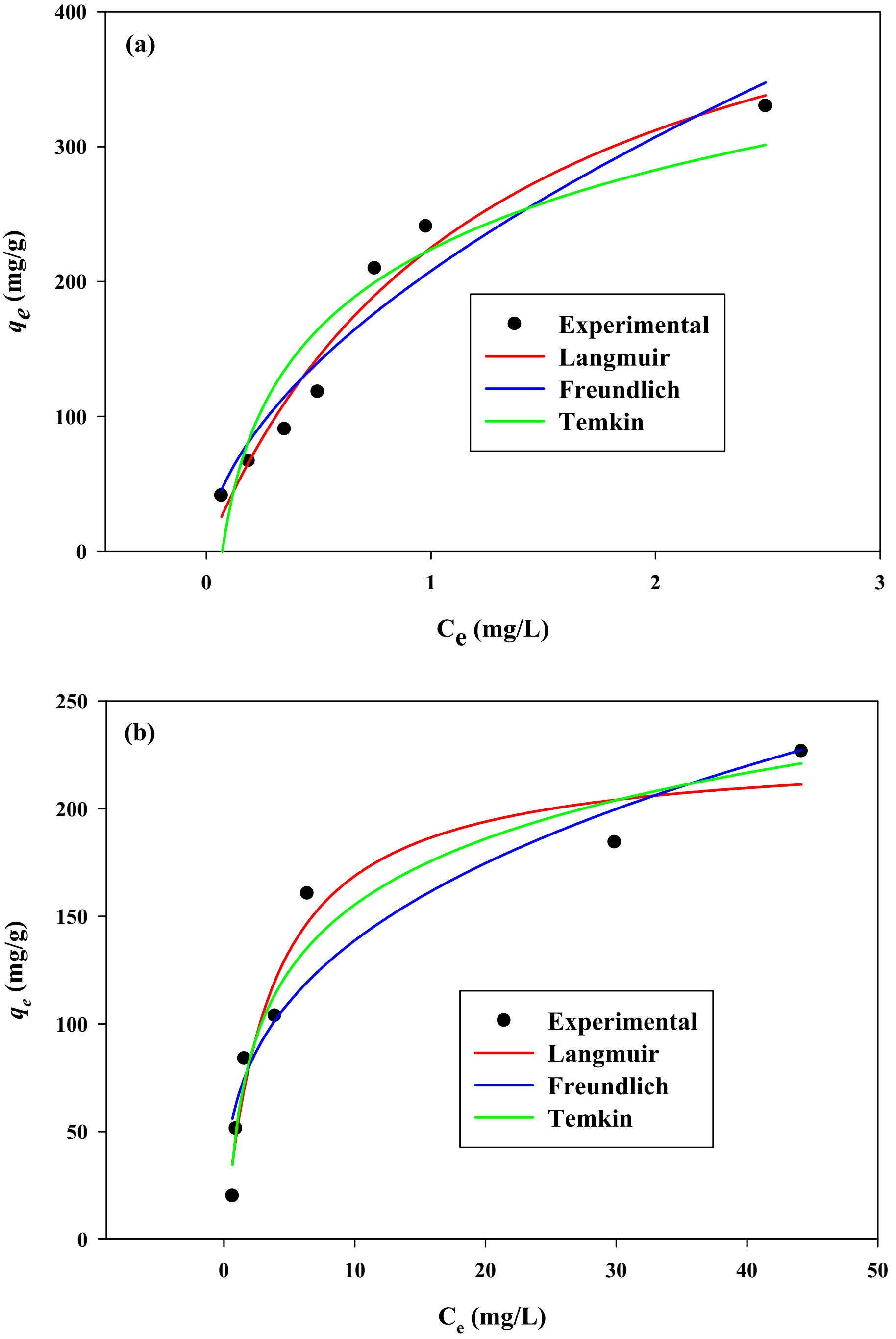

Fig. 9 Adsorption isotherms of (**a**) BG1 (dosage = 0.08 g, solution pH = 9, temperature = 25 °C, agitation speed = 85 rpm, and volume of solution = 100 mL) and (**b**) RB19 (dosage = 0.08 g, solution pH = 4, temperature = 25 °C, agitation speed = 85 rpm, and volume of solution = 100 mL)

Plotting ln k_d vs. 1/T (Fig. 10) allows to compute ΔS^{o} and ΔH^{o} parameters, where slope represents ΔH^{o}, while intercept signifies ΔS^{o}. Table 9 displays the results derived from thermodynamic factors. The negative numbers of ΔG° reflect the spontaneity of BG1 and RB19 adsorption by the CHI/MMT/ALG, which might be thermodynamically desirable. Furthermore, the endothermic nature of the BG1 and RB19 adsorption by CHI/MMT/ALG was confirmed by the positive values of ΔH^{o} (156.99 kJ/mol for BG1 and 160.11 kJ/mol for RB19) [62]. The elevation in irregularity at the adsorbent-liquid interface caused by the uptake of BG1 and RB19 molecules onto the CHI/MMT/ALG surface is illustrated by the positive values of ΔS^{o} (0. 543 kJ/mol K for BG1 and 0.535 kJ/mol K for RB19).

Adsorption Mechanism of Dyes

There are several functional groups present on the surface of the CHI/MMT/ALG, which are evidenced via FTIR analysis. These data were used to construct the adsorption

Table 8 Comparison of the adsorption capacity of CHI/MMT/ALG towards BG1 and RB19 dyes with different adsorbents

Adsorbents	Dye	q_{max} (mg/g)	References
CHI/MMT/ALG	BG1	509.5	This study
CHI/MMT/ALG	RB19	227.9	This study
Graphite oxide nanoparticle	BG	416.67	[53]
Hemp hurd nanocomposite	BG	256	[54]
Chitosan-graft-itaconic acid	BG	135	[55]
Nano hydroxyapatite/chitosan composite	BG	49.1	[56]
Chitosan hollow fibers	RB19	454.5	[57]
ZnO-polyacrylonitrile-hinokitiol	RB19	267.37	[58]
Cross-linked glutaraldehyde-chitosan/MgO/Fe_3O_4	RB19	193.2	[19]
Nano-carbon material	RB19	116.01	[59]
Hybrid magnetic $CoFe_2O_4$@γ-Fe_2O_3@CTAB nanocomposite	RB19	56.3	[60]

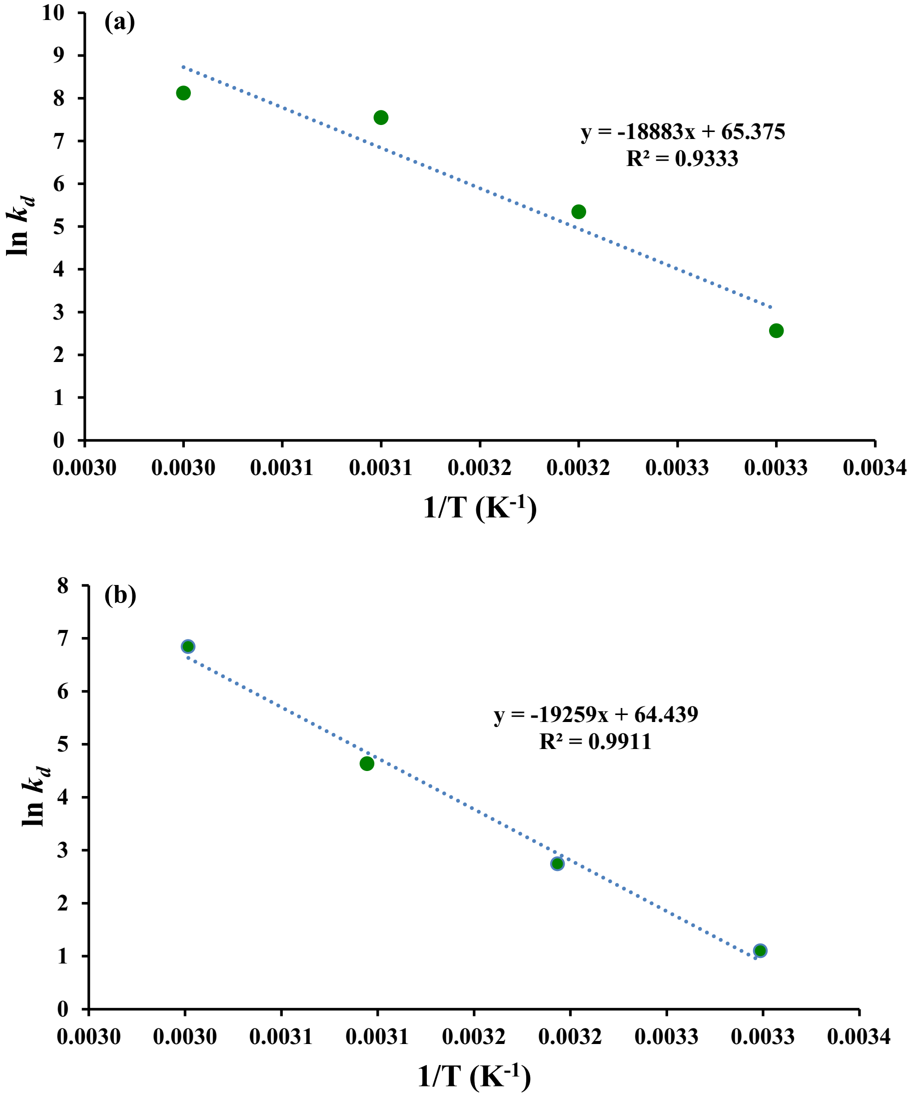

Fig. 10 Van't Hoff plot for (**a**) BG1 and (**b**) RB19 adsorption onto CHI/MMT/ALG (dosage = 0.08 g, solution pH = 9 for BG1 and 4 for RB19, agitation speed = 85 rpm, and volume of solution = 100 mL)

Table 9 Thermodynamic parameters for the adsorption of BG1 and RB19 on CHI/MMT/ALG

	T (K)	k_d	ΔG° (kJ/mol)	ΔH° (kJ/mol)	ΔS° (kJ/molK)
BG1	303.15	12.937	− 6.45	156.99	0.543
	313.15	209.17	− 13.91		
	323.15	1892.4	− 20.25		
	333.15	3362.2	− 22.65		
RB19	303.15	3.0035	− 2.74	160.11	0.535
	313.15	15.514	− 7.13		
	323.15	102.87	− 12.43		
	333.15	935.76	− 17.56		

mechanisms for the cationic dye (BG1) and the anionic dye (RB19), as depicted in Fig. 11. The active groups that can adsorb both cationic and anionic contaminants are very numerous in CHI/MMT/ALG, as mentioned earlier, making it a super absorbent material known as a zwitterion adsorbent. The CHI/MMT/ALG's composition of inorganic materials (MMT) and biomaterials (CHI and ALG), both of which are naturally rich in active groups. In this way, the active groups of CHI/MMT/ALG, which are $–NH_2$, PO_4^{-3}, –COOH, -OH, and ≡Si–OH, allow CHI/MMT/ALG to effectively remove BG1 dye in the alkaline medium via the electrostatic interactions between the negative groups $(PO_4^{-3}, \equiv Si-O^-, -COO^-, \text{ and } -O^-)$ of the CHI/MMT/ALG and the dependent group $\left(=N^+-\left(CH_2CH_3\right)_2\right)$ of the BG1 [31, 38]. Conversely, in the acidic media, the CHI/MMT/ALG adsorbs the RB19 by electrostatic interactions between the sulfonate groups $(-SO_3^-)$ of the RB19 and the protonated groups of the CHI/MMT/ALG [19]. Due to a large number of hydroxyl groups on the surface of CHI/MMT/ALG, which supplies considerable hydrogen to form hydrogen bonds with the N and O atoms of adsorbates. The connection between the aromatic rings of the BG1 and RB19 dyes and the nitrogen and oxygen groups in CHI/MMT/ALG generates n-π interactions, which assist in the adsorption process of both dyes. Finally, the exchangeable cations present in MMT of CHI/MMT/ALG can be exchanged with BG1 cations through ion exchange.

Conclusion

A green and eco-friendly biomaterial of CHI/MMT/ALG composite was effectively developed to be an alternative adsorbent to remove dyestuffs including BG1 and RB19 from the aqueous solutions. Based on the BBD model,

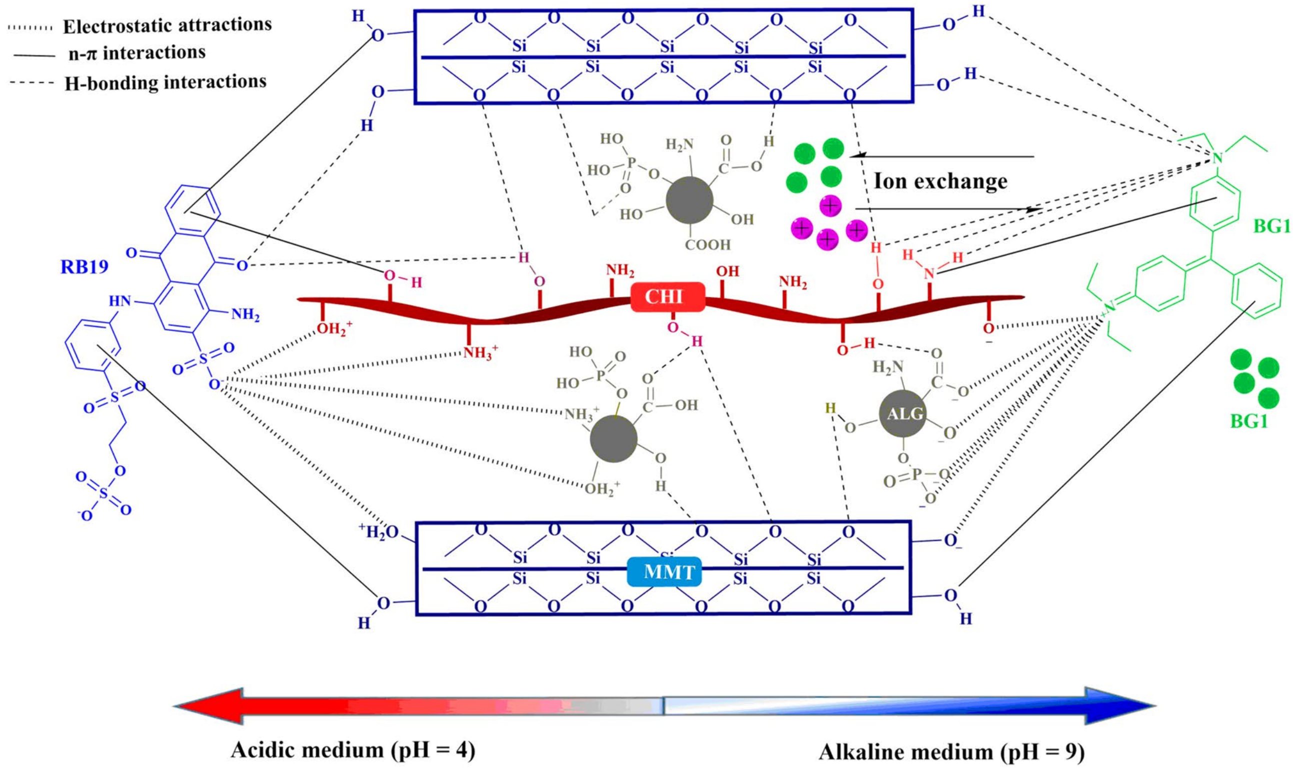

Fig. 11 Illustration of the possible interaction among CHI/MMT/ALG and dyes (BG1 and RB19), namely, electrostatic interactions, hydrogen bonding, n-π stacking, and ion exchange

maximum removals of 76.2% and 91.7% were attained at CHI/MMT/ALG dosage of 0.08 g, pH of 9 for BG1 and 4 for RB19, and duration of 17.5 min for BG1 and RB19, respectively. The equilibrium and kinetic findings revealed that the adsorption of BG1 and RB19 happened via monolayer adsorption, with chemisorption functioning as the rate-controlling step. Thermodynamic calculations demonstrated that the adsorption process of BG1 and RB19 was favorable and spontaneous. The maximum adsorption capacity of CHI/MMT/ALG for BG1 and RB19 was specified to be 509.5 mg/g and 227.9 mg/g, respectively. The improved surface functionalities of CHI/MMT/ALG inspired the adsorption mechanism of CHI/MMT/ALG for BG1 and RB19 could be essentially ascribed by electrostatic attraction, n-π stacking, and hydrogen bonding. The results of the investigation show that the newly formed CHI/MMT/ALG has a large potential for use in wastewater treatment systems.

Acknowledgements The authors are thankful to the Faculty of Applied Sciences, Universiti Teknologi MARA (UiTM) Shah Alam, Malaysia for the research facilities. The author (Zeid A. ALOthman) is grateful to the Researchers Supporting Project No. (RSP2023R1), King Saud University, Riyadh, Saudi Arabia.

Authors Contributions All authors contributed to the study conception and design. Material preparation, data collection and analysis were performed by KR, ASA, SNS, ZAA, AHJ. The first draft of the manuscript was written by KR, ASA, AHJ, and all authors commented on previous versions of the manuscript. All authors read and approved the final manuscript.

Funding The author (Zeid A. ALOthman) is grateful to the Researchers Supporting Project No. (RSP2023R1), King Saud University, Riyadh, Saudi Arabia.

Data Availability The datasets used and/or analyzed during the current study are available from the corresponding author on reasonable request.

Declarations

Competing Interests The authors declare that they have no competing interests.

Ethical Approval Not applicable.

Consent to Participate Not applicable.

Consent to Publish Not applicable.

References

1. Eltabey RM, Abdelwahed FT, Eldefrawy MM, Elnagar MM (2022) Fabrication of poly (maleic acid)-grafted cross-linked chitosan/montmorillonite nanospheres for ultra-high adsorption of anionic acid yellow-17 and cationic brilliant green dyes in single and binary systems. J Hazard Mater 439:129589
2. Tkaczyk A, Mitrowska K, Posyniak A (2020) Synthetic organic dyes as contaminants of the aquatic environment and their implications for ecosystems: a review. Sci Total Environ 717:137222
3. Akar ST, Koc E, Sayin F, Kara I, Akar T (2021) Design and modeling of the decolorization characteristics of a regenerable and eco-friendly geopolymer: batch and dynamic flow mode treatment aspects. J Environ Manage 298:113548
4. Tripathy BK, Kumar S, Kumar M, Debnath A (2020) Microwave induced catalytic treatment of brilliant green dye with carbon doped zinc oxide nanoparticles: central composite design, toxicity assessment and cost analysis. Environ Nanotechnol Monit Manage 14:100361
5. Zhang L, Su M, Guo X (2008) Studies on the treatment of brilliant green solution by combination microwave induced oxidation with $CoFe_2O_4$. Sep Purifi Technol 62(2):458–463
6. Reghioua A, Barkat D, Jawad AH, Abdulhameed AS, Khan MR (2021) Synthesis of Schiff's base magnetic crosslinked chitosan-glyoxal/ZnO/Fe_3O_4 nanoparticles for enhanced adsorption of organic dye: modeling and mechanism study. Sustain Chem Pharm 20:100379
7. Chen M, Yang H, Xu ZL, Cheng C (2022) Separation of single and mixed anionic dyes in saline solutions using uncharged polyacrylonitrile-tris (hydroxymethyl) aminomethane (PAN-Tris) ultrafiltration membrane: performance and mechanism. J Clean Prod 336:130471
8. Nnaji PC, Anadebe VC, Ezemagu IG, Onukwuli OD (2022) Potential of *Luffa cylindrica* seed as coagulation-flocculation (CF) agent for the treatment of dye wastewater: kinetic, mass transfer, optimization and CF adsorption studies. Arab J Chem 15(2):103629
9. Sayin F (2022) Insight into decolorization characteristics of a green biocomposite sorbent system prepared by immobilization of fungal cells on lignocellulosic matrix: Box-behnken design. Water Air Soil Pollut 233(7):262
10. Sánchez-Albores R, Cano FJ, Sebastian PJ, Reyes-Vallejo O (2022) Microwave-assisted biosynthesis of ZnO-GO particles using orange peel extract for photocatalytic degradation of methylene blue. J Environ Chem Eng 10(6):108924
11. Singh AL, Chaudhary S, Kumar S, Kumar A, Singh A, Yadav A (2022) Biodegradation of reactive yellow-145 azo dye using bacterial consortium: a deterministic analysis based on degradable Metabolite, phytotoxicity and genotoxicity study. Chemosphere 300:134504
12. Pormazar SM, Dalvand A (2022) Adsorption of reactive black 5 azo dye from aqueous solution by using amine-functioned Fe_3O_4 nanoparticles with L-arginine: process optimisation using RSM. Int J Environ Anal Chem 102(8):1764–1783
13. Russo T, Fucile P, Giacometti R, Sannino F (2021) Sustainable removal of contaminants by biopolymers: a novel approach for wastewater treatment. Curr State Futur Perspect Process 9(4):719
14. Omer AM, Dey R, Eltaweil AS, Abd El-Monaem EM, Ziora ZM (2022) Insights into recent advances of chitosan-based adsorbents for sustainable removal of heavy metals and anions. Arab J Chem 15(2):103543
15. Shahadat M, Jha A, Islam SU, Ali SW, Ahammad SZ, Adnan R, Ismail I (2022) Recent advances in chitosan-polyaniline based nanocomposites for environmental applications: a review. Polymer. https://doi.org/10.1016/j.polymer.2022.124975
16. Abdulhameed AS, Jawad AH, Vigneshwaran S, ALOthman ZA, Yaseen ZM (2022) Different TiO_2 phases (Degussa/Anatase) modified cross-linked chitosan composite for the removal of reactive red 4 dye: Box-behnken design. J Polym Environ 30(12):5084–5099
17. Hamza MF, Wei Y, Mira HI, Adel AH, Guibal E (2019) Synthesis and adsorption characteristics of grafted hydrazinyl amine magnetite-chitosan for Ni (II) and Pb (II) recovery. Chem Eng J 362:310–324

18. Ibrahiem HA, El-Dougdoug WI, Hefni HH, El-Sawy AA, Kamal HM, Mahmoud KF (2021) Removal of Ni (II), Mn (II) and Zn (II) from crude yellow cake aqueous solution by cross-linked chitosan and polyvinyl alcohol. Egypt J Petrol 30(3):61–69
19. Jawad AH, Rangabhashiyam S, Abdulhameed AS, Syed-Hassan SSA, ALOthmanWilson ZALD (2022) Process optimization and adsorptive mechanism for reactive blue 19 dye by magnetic crosslinked chitosan/MgO/Fe_3O_4 biocomposite. J Polym Environ 30(7):2759–2773
20. Zaman HG, Baloo L, Aziz F, Kutty SR, Ashraf A (2022) COD adsorption and optimization from produced water using chitosan–ZnO nanocomposite. Appl Nanosci 12(6):1885–1898
21. Ye X, Shang S, Zhao Y, Cui S, Zhong Y, Huang L (2021) Ultra-efficient adsorption of copper ions in chitosan–montmorillonite composite aerogel at wastewater treatment. Cellulose 28(11):7201–7212
22. Saad EM, Elshaarawy RF, Mahmoud SA, El-Moselhy KM (2021) New ulva lactuca algae based chitosan bio-composites for bioremediation of Cd (II) ions. J Bioresour Bioprod 6(3):223–242
23. Kurczewska J (2022) Chitosan-montmorillonite hydrogel beads for effective dye adsorption. J Water Process Eng 48:102928
24. Wang W, Fan M, Ni J, Peng W, Cao Y, Li H, Song S (2022) Efficient dye removal using fixed-bed process based on porous montmorillonite nanosheet/poly (acrylamide-co-acrylic acid)/sodium alginate hydrogel beads. Appl Clay Sci 219:106443
25. Miao Y, Peng W, Wang W, Cao Y, Li H, Chang L, Zhang T (2022) 3D-printed montmorillonite nanosheets based hydrogel with biocompatible polymers as excellent adsorbent for Pb (II) removal. Sep Purifi Technol 283:120176
26. Kang S, Zhao Y, Wang W, Zhang T, Chen T, Yi H, Song S (2018) Removal of methylene blue from water with montmorillonite nanosheets/chitosan hydrogels as adsorbent. Appl Surf Sci 448:203–211
27. Wang W, Ni J, Chen L, Ai Z, Zhao Y, Song S (2020) Synthesis of carboxymethyl cellulose-chitosan-montmorillonite nanosheets composite hydrogel for dye effluent remediation. Int J Biol Macromol 165:1–10
28. Ting ASY, Cheng CKW, Santiago KAA (2021) Decolourization of malachite green dye by endolichenic fungi from the lichen Usnea sp.: a novel study on their dye removal potential. J King Saud Uni-Sci 33(7):101579
29. Ramachandran G, Chackaravarthi G, Rajivgandhi GN, Quero F, Maruthupandy M, Alharbi NS, Li WJ (2022) Biosorption and adsorption isotherm of chromium (VI) ions in aqueous solution using soil bacteria *Bacillus amyloliquefaciens*. Environ Res 212:113310
30. Hockaday J, Harvey A, Velasquez-Orta S (2022) A comparative analysis of the adsorption kinetics of Cu^{2+} and Cd^{2+} by the microalgae *Chlorella vulgaris* and *Scenedesmus obliquus*. Algal Res 64:102710
31. Abdulhameed AS, Jawad AH, Kashi E, Radzun KA, ALOthman-Wilson ZALD (2022) Insight into adsorption mechanism, modeling, and desirability function of crystal violet and methylene blue dyes by microalgae: Box-Behnken design application. Algal Rese 67:102864
32. Zain ZM, Abdulhameed AS, Jawad AH, ALOthman ZA, Yaseen ZM (2022) A pH-sensitive surface of chitosan/sepiolite clay/algae biocomposite for the removal of malachite green and remazol brilliant blue R dyes: optimization and adsorption mechanism study. J Polym Environ. https://doi.org/10.1007/s10924-022-02614-y
33. Dalvand A, Nabizadeh R, Ganjali MR, Khoobi M, Nazmara S, Mahvi AH (2016) Modeling of reactive blue 19 azo dye removal from colored textile wastewater using L-arginine-functionalized Fe_3O_4 nanoparticles: optimization, reusability, kinetic and equilibrium studies. J Magne Magne Mater 404:179–189
34. Sing KS (1985) Reporting physisorption data for gas/solid systems with special reference to the determination of surface area and porosity (Recommendations 1984). Pure Appl Chem 57(4):603–619
35. Ma L, Zhou X, Xu L, Xu X, Zhang L, Chen W (2015) Chitosan-assisted fabrication of ultrathin MoS_2/graphene heterostructures for Li-ion battery with excellent electrochemical performance. Electrochim Acta 167:39–47
36. Lazaridou M, Nanaki S, Zamboulis A, Papoulia C, Chrissafis K, Klonos PA, Bikiaris DN (2021) Super absorbent chitosan-based hydrogel sponges as carriers for caspofungin antifungal drug. Int J Pharm 606:120925
37. Chen YW, Lee HV, Juan JC, Phang SM (2016) Production of new cellulose nanomaterial from red algae marine biomass Gelidium elegans. Carbohydr Polym 151:1210–1219
38. Altıntıg E, Ates A, Angın D, Topal Z, Aydemir Z (2022) Kinetic, equilibrium, adsorption mechanisms of RBBR and MG dyes on chitosan-coated montmorillonite with an ecofriendly approach. Chem Eng Res Design 188:287–300
39. Almomani F, Bhosale RR (2021) Bio-sorption of toxic metals from industrial wastewater by algae strains Spirulina platensis and *Chlorella vulgaris*: application of isotherm, kinetic models and process optimization. Sci Total Environ 755:142654
40. Jawad AH, Abdulhameed AS, Wilson LD, Hanafiah MAKM, Nawawi WI, ALOthman ZA, RizwanKhan M (2021) Fabrication of Schiff's base chitosan-glutaraldehyde/activated charcoal composite for cationic dye removal: optimization using response surface methodology. J Polym Environ 29:2855–2868
41. Kutluay S, Temel F (2021) Silica gel based new adsorbent having enhanced VOC dynamic adsorption/desorption performance. Colloids Surf A: Physicochem Eng Asp 609:125848
42. Marichamy MK, Kumaraguru A, Jonna N (2021) Particle size distribution modeling and kinetic study for coagulation treatment of tannery industry wastewater at response surface optimized condition. J Clean Prod 297:126657
43. Pandey S, Son N, Kang M (2022) Synergistic sorption performance of karaya gum crosslink poly (acrylamide-co-acrylonitrile)@ metal nanoparticle for organic pollutants. Int J Biol Macromol 210:300–314
44. Lagergren S (1898) Zur theorie der sogenannten adsorption geloster stoffe. Vet Akad Handl 24:1–39
45. Ho YS, McKay G (1998) Sorption of dye from aqueous solution by peat. Chem Eng J 70:115–124
46. Wang Z, Liu L, Lan Y, Li W (2022) Sn0-modified carbon derived from cigarette butts as a recycled material for enhanced removal of antibiotic phenacetin. J Environ Chem Eng 10(2):107164
47. Normi NI, Abdulhameed AS, Jawad AH, Surip SN, Razuan R, Ibrahim ML (2022) Hydrothermal-assisted grafting of Schiff base Chitosan by Salicylaldehyde for adsorptive removal of acidic dye: statistical modeling and adsorption mechanism. J Polym Environ. https://doi.org/10.1007/s10924-022-02730-9
48. Langmuir I (1918) The adsorption of gases on plane surfaces of glass, mica and platinum. J Am Chem Soc 40:1361–1403
49. Frendlich HMF (1906) Over the adsorption in solution. J Phys Chem 57:385–471
50. Temkin MI (1940) Kinetics of ammonia synthesis on promoted iron catalysts, Acta physiochim. URSS 12:327–356
51. Li C, Zhao S, Huang X, Xie D, Li X, Ma J, Liao Y (2022) Development of humic acid based adsorbents for fast and efficient removal of ammonia and organic nitrogen from super magnetic separation treated wastewater. J Environ Chem Eng 10(2):107223
52. Hoseinzadeh H, Hayati B, Ghaheh FS, Seifpanahi-Shabani K, Mahmoodi NM (2021) Development of room temperature synthesized and functionalized metal-organic framework/graphene oxide composite and pollutant adsorption ability. Mater Res Bullet 142:111408

53. Ghaedi M, Zeinali N, Ghaedi AM, Teimuori M, Tashkhourian J (2014) Artificial neural network-genetic algorithm based optimization for the adsorption of methylene blue and brilliant green from aqueous solution by graphite oxide nanoparticle. Spectrochimica Acta Part A: Mol Biomol Spectro 125:264–277
54. Mandal S, Alankar T, Hughes R, Marpu SB, Omary MA, Shi SQ (2022) Removal of hazardous dyes and waterborne pathogens using a nanoengineered bioadsorbent from hemp–fabrication, characterization and performance investigation. Surf Interface 29:101797
55. Özkahraman B, Bal A, Acar I, Güçlü G (2011) Adsorption of brilliant green from aqueous solutions onto crosslinked chitosan graft copolymers. Clean-Soil Air Water 39(11):1001–1006
56. Ragab A, Ahmed I, Bader D (2019) The removal of brilliant green dye from aqueous solution using nano hydroxyapatite/chitosan composite as a sorbent. Mol 24(5):847
57. Mirmohseni A, Dorraji MS, Figoli A, Tasselli F (2012) Chitosan hollow fibers as effective biosorbent toward dye: preparation and modeling. Biores Technol 121:212–220
58. Phan DN, Rebia RA, Saito Y, Kharaghani D, Khatri M, Tanaka T, Kim IS (2020) Zinc oxide nanoparticles attached to polyacrylonitrile nanofibers with hinokitiol as gluing agent for synergistic antibacterial activities and effective dye removal. J Ind Eng Chem 85:258–268
59. Liang C, Shi Q, Feng J, Yao J, Huang H, Xie X (2022) Adsorption behaviors of cationic methylene blue and anionic reactive blue 19 dyes onto nano-carbon adsorbent carbonized from small precursors. Nanomater 12(11):1814
60. Oliveira HALD, Gomide G, Vieira CADM, Guerra AAAM, Depeyrot J, Campos AFC (2022) Hybrid magnetic $CoFe_2O_4@\gamma\text{-}Fe_2O_3@CTAB$ nanocomposites as efficient and reusable adsorbents for Remazol Brilliant Blue R dye. Environ Technol. https://doi.org/10.1080/09593330.2022.2115946
61. Gao M, Xu D, Gao Y, Chen G, Zhai R, Huang X, Liu G (2021) Mussel-inspired triple bionic adsorbent: facile preparation of layered double hydroxide@ polydopamine@ metal-polyphenol networks and their selective adsorption of dyes in single and binary systems. J Hazard Mater 420:126609
62. Ahmad R, Ansari K (2022) Fabrication of alginate@ silver nanoparticles (Alg@AgNPs) bionanocomposite for the sequestration of crystal violet dye from aqueous solution. Int J Biol Macromol 218:157–167